SENSITIVITY TESTING OF A NEW MODEL WITH SPECIAL OBSERVATIONS

Jan Paegle (U. of Utah, jpaegle@met.utah.edu), Lee Byerle (U..S.A.F), Juan Ruiz, Celeste Saulo (CIMA, U. of Buenos Aires), Julia Nogues Paegle (U. of Utah)

1. Introduction

How can we estimate the value of new atmospheric observations for weather prediction? One way is to determine whether new observations improve weather forecasts, or whether new observations have any impact on the forecasts. This depends upon the type and quantitity of observations. It also depends upon the models performing the forecasts. The purpose of the presentation is to point out that different models exhibit substantially different sensitivity to insertion of new observations.

It would be best to perform analyses of observational utility with the most complete models used operationally at ECMWF or NCEP. Unfortunately, such models are too expensive to run at full resolution in small research environments including university departments. In such environments, the question of forecast sensitivity to observations can be approached only with lower resolution models or with models that cover relatively restricted domains.

Early sensitivity experiments were conducted in the context of atmospheric predictability. Thompson (1957) studied predictability with a simple barotropic model in a bounded domain, and Lorenz (1969) expanded on the approach with a periodic domain. Lorenz (1969) estimated the spectra of atmospheric motions and of their uncertainty and concluded that the larger scales of atmospheric flows might be deterministically predictable for a period on the order of a couple of weeks. After a few weeks, relatively small uncertainties of the initial state produce forecast uncertainties that are as large as the differences of arbitrarily selected weather states.

These results have been approximately supported in many studies performed with dynamically more complete models. Such models are initialized with estimates of the initial state made from observations and perturbations of the initial state based upon modern estimates of observational uncertainty. Miguez-Macho and Paegle (2000), for example, used retrospective reanalyses of atmospheric states produced by two equally credible analysis systems and determined that the resulting forecasts were similar at short times, but diverged with forecast time. The spectral decomposition of error growth suggested an evolution similar to one originally predicted by Thompson's (1957) study. This and the fact that the primitive equation model used by Miguez-Macho and Paegle (2000) exhibited similar skill as the NCEP global model run at similar resolution (truncated at approximately wavenumbers 40-60) lent confidence to their results.

More recent experiments using the same model at higher wavenumber 84 resolution (Roman et al. 2004) suggest greater forecast sensitivity to smaller scales than allowed in Miguez-Macho and Paegle's (2000) experiments, but these global experiments could not be expanded to yet higher resolution because of

computer resource limitations. The results suggest forecast sensitivity not only to initial state differences but also to model resolution and thereby imply that predictability conclusions may be influenced by model configuration.

Our present purpose is to more systematically study the sensitivity of atmospheric predictability to models and to present a relatively affordable strategy to study predictability in a global model using variable resolution. We begin with an outline of the dynamical formulations that have been most commonly used to study atmospheric predictability in section 2. Section 3 follows with a description of two possible initial state specifications that use and disregard experimental observations made in a region of the world whose operational observational coverage is poor. Section 4 presents forecast sensitivity of different models to the extra data, Section 5 presents more detailed study of forecast sensitivity to initial state changes and Section 6 summarizes conclusions.

2. Models

The earliest predictability studies (e.g.,Thompson, 1957, Lorenz, 1969) were based upon the barotropic forecast model and the following equations:

$\partial\zeta/\partial t = -\nabla_H\cdot(V(\zeta+f))$
$\nabla^2\Psi=\zeta$
$u=-\partial\Psi/\partial y;\ v=\partial\Psi/\partial x$

Here, ζ is relative vorticity, f is Coriolis parameter, V is the wind vector,$\Psi$is streamfunction, and u and v are eastward and westward wind components, respectively. Time, eastward and northward distances are denoted by t, x, y, and $\nabla_H$is the horizontal gradient operator. This forecast model has only one forecast equation, it applies to a horizontal domain, and allows only energy propagation by horizontal advection and Rossby wave propagation. This permits relatively large time steps and produces efficient forecast algorithms. Thompson's (1957) and Lorenz's (1969) predictability studies were based upon simplified versions of this model.

Many more recent predictability studies are based upon the primitive equations, listed below:

$\partial u/\partial t=-V\cdot\nabla u+fv-g\partial Z/\partial x+\nabla_H\cdot(K_H\nabla_H u)+\partial(K_Z\partial u/\partial z)/\partial z$
$\partial v/\partial t=-V\cdot\nabla v-fu-g\partial Z/\partial y+\nabla_H\cdot(K_H\nabla_H v)+\partial(K_Z\partial v/\partial z)/\partial z$
$\partial\Theta/\partial t=-V\cdot\nabla\Theta+\nabla_H\cdot(K_H\nabla_H\Theta)+\partial(K_Z\partial\Theta/\partial z)/\partial z$ +Heating
$\partial q/\partial t=-V\cdot\nabla q+\nabla_H\cdot(K_H\nabla_H q)+\partial(K_Z\partial q/\partial z)/\partial z$ - Condensation+Evaporation
$\partial\omega/\partial p=-\nabla_H\cdot(V_H)$
$\partial Z/\partial p=-RT/(Pg)$

Here ∇represents the three-dimensional gradient operator, V is the three dimensional velocity vector, $V_H$is the horizontal velocity vector, $\Theta$is potential temperature, T is temperature, ω is vertical motion in pressure coordinates, q is specific humidity, $\alpha$is specific volume, p is pressure, g is apparent gravitation, R is the gas constant, Z is geopotential height, and z is geometrical height. K_H and $K_Z$are horizontal and vertical diffusivity, and horizontal diffusion is here

written in second order, Laplacian form. Some models also include higher order horizontal diffusion. Diffusion terms remove amplitude from all cases, but do so more strongly at smaller scales, particularly for higher order approaches.

The primitive equations contain 4 forecast equations, 6 dependent variables, and are solved in a three dimensional domain. They permit energy propagation by Rossby waves and by horizontally propagating gravity waves. The resulting algorithm requires smaller time steps and substantially more computational effort than the barotropic model. Primitive equation models have been used in numerous predictability studies (e.g. Miguez-Macho and Paegle, 2000, 2001; Tribbia and Baumhefner, 2004, Roman et al., 2004 for recent results).

The system of Euler equations constitutes the most complete dynamical core commonly used for atmospheric prediction. This model retains Rossby, gravity, and acoustic waves, and the gravity and acoustic modes propagate in all three spatial dimensions. The governing equations can be written in the following form.

$\partial u/\partial t$=-V$\cdot\nabla$u+fv-$\alpha\partial P/\partial x+\nabla_H \cdot (K_H \nabla_H u)+\partial(K_Z \partial u/\partial z)/\partial z$
$\partial v/\partial t$=-V$\cdot\nabla$v-fu-$\alpha\partial P/\partial y+\nabla_H \cdot (K_H \nabla_H v)+\partial(K_Z \partial v/\partial z)/\partial z$
$\partial\Theta/\partial t$=-V$\cdot\nabla\Theta+\nabla_H \cdot (K_H \nabla_H \Theta)+\partial(K_Z \partial\Theta/\partial z)/\partial z$ +Htg
$\partial q/\partial t$=-V$\cdot\nabla q+\nabla_H \cdot (K_H \nabla_H q)+\partial(K_Z \partial q/\partial z)/\partial z$ -Condensation+Evaporation
$\partial w/\partial t$=-V$\cdot\nabla$w+Coriolis-$\alpha\partial P/\partial z+\nabla_H \cdot (K_H \nabla_H w)+\partial(K_Z \partial w/\partial z)/\partial z$-g
$\partial P/\partial t$=-V$\cdot\nabla$P-γP$\nabla\cdot$V

Here, w is vertical velocity in height coordinates, P is pressure, γ is 1.4. Diffusivity is written in second order form, but other higher order diffusivity formulations can be used. There are 6 forecast variables, and small time steps must be used for numerical stability. The latter constraint is particularly severe in the vertical dimension, which in many models is treated with semi-implicit time differencing schemes. These schemes distort acoustic wave propagation in the vertical direction, but presumably do not seriously affect other modes of energy propagation.

Forecasts made by the primitive equation and Euler models are influenced by parameterization of sub-grid scale turbulent mixing, simulated by K_H and K_Z terms. Vertical diffusion terms produce second order vertical derivatives with respect to z in the forecast equations. Such terms are required in order to satisfy boundary conditions specified on forecast variables at the model top and bottom boundaries. Fairly reasonable formulations are available for $K_Z$based upon turbulence closure models, and these can be indirectly validated, at least near the lower model boundaries by comparisons of observed and simulated vertical profiles and surface fluxes.

Formulations for K_H are more abritrary but horizontal diffusion is often included to maintain numerical stability or to inhibit "noisy" forecasts, (e.g. Knievel et al., 2005 and Skamarock and Baldwin, 2003). It was necessary to include both second and fourth order horizontal diffusion in the primitive equation model used in predictability studies of Miguez-Macho and Paegle (2000, 2001) and Roman et al. (2004). The selected diffusivities were similar to those present

in early versions of the NCAR Community Climate Model that was in common use about 10-20 years ago. The resulting forecasts were similar to those produced at similar resolution by operational NCEP models (Miguez-Macho and Paegle, 2000), but this does not prove that the selected horizontal diffusion was correct.

Uniform resolution versions of our recent Euler model are typically stable for 2 week predictions without any horizontal diffusion, and occasional instabilities that occur later in such forecasts are controlled by implementation of divergence diffusion in the upper model levels above approximately 14 km. The resulting forecasts develop substantial detail in smaller resolved scales, and also produce greater forecast sensitivity to the initial state than does our global primitive equation model.

3. Initial State Specifications

The initial states selected for present experimentation cover the period from 15 Dec. 2002 to 15 Feb. 2003. During this time the South American Low-Level Jet Experiment (SALLJEX) was executed in a region centered over the eastern foothills of the central Andes Mountains (Vera et al., 2006). The area of upper air observation enhacement during SALLJEX extends from approximately 30^0S to 10^0S and 69^0W to 54^0W (see Fig. 4 of Vera et al., 2006). Here, additional radiosonde and pibal observations were made 2 to 4 times a day in a region that was previously a near data void in the operational above-surface observing network.

Dirceu et al. (2007) performed several global analyses during this period. One analysis ("control") employed the operational global analysis system ("GDAS") that is used to initialize global model forecasts at the National Centers for Atmospheric Prediction (NCEP) and included only the operational observing network. A second analysis ("experiment") was identical, but also included the additional SALLJEX upper air observations. Both analyses were output at 6h intervals on a 1^0X 1^0 latitude longitude grid on 26 vertical levels extending from 1000 mb to 10 mb.

Figure 1 presents a sample difference field between experiment and control analyses wind fields, valid for 00UTC on 24 January. Figure 2 displays the time series of rms differences between control and experiment 500 mb wind analyses, averaged over the domain displayed in Fig. 1. The SALLJEX observations appear to have maximum influence upon the analyses in the last half of January 2003. This is also a period of several interesting weather events and intensive observing periods during which the SALLJEX observing frequency and coverage were augmented. For these reasons, much of the subsequent analysis emphasizes forecasts initialized in the period starting on 15 January and ending on 30 January.

4. Forecast sensitivity to SALLJEX observations

The impact of SALLJEX observations upon numerical prediction is here studied with four different models. The first is a global primitive equation model developed at the University of Utah and referred to as the Utah Global Model (UGM). It is similar to the primitive equation model outlined in Section 2, but forecasts the vertical component of vorticity and horizontal divergence

rather than the horizontal wind. The results are mathematically equivalent to the version outlined in Section 2, but certain practical numerical considerations, such as the time split treatment of rapidly propagating gravity waves are facilitated in the UGM. The present UGM integrations are performed on a latitude-longitude grid retaining 82 points in latitude and 128 points in longitude and 20 levels in the vertical using a time step of 900 seconds for most variables. Rapidly propagating, deep gravity waves are integrated with a smaller time step via time splitting. The model development is outlined by Paegle (1989) and it has been used in several predictability studies (e.g. Miguez-Macho and Paegle, 2000, 2001, Byerle and Paegle (2004), and Roman et al. (2004)). The anomaly correlations of the UGM executed at present resolutions are similar to those produced by the Medium Range Forecasts of NCEP that are part of the NCEP reanalysis archive and integrated with wavenumber 64 resolution (Miguez-Macho and Paegle, 2000).

The second model is a global Euler model also developed at the University of Utah. The model development is outlined by Roman (2004). Preliminary testing is described by Roman (2004) who shows that this model has similar error characteristics as the UGM when both are run at the same resolution. The global Euler model is executed at the same resolution as the UGM, and uses a 100s time step. This is substantially shorter than the time step used in the primitive equation model and this is a disadvantage of the present global Euler model. The main advantage of the global Euler model is that it can be executed with relatively small amounts of diffusion. This, and the more general dynamical treatment allow stronger forecast sensitivity to initial state changes. This model is executed in uniform and variable resolution grids, described below.

The third model used in the intercomparison is a regional version of the Weather and Research Forecast (WRF) model. The WRF model is based upon a version of the Euler equations applied to a regional domain. The WRF model was been developed in a broad community collaboration, and it has undergone extensive sensitivity testing. Present applications are run on the regional domain displayed in Fig. 1, using 50 km grid size. This time step is relatively large compared to that used in the lower resolution global Euler model because the WRF model contains sophisticated numerical methods designed to treat horizontal acoustic wave propagation in an efficient time split approach. These methods have not been incorporated in the present global Euler model. The WRF model uses Grell convective parameterization and Mellor-Yamada treatment of boundary layer processes. The Grell parameterization of convection is more complete than the convective adjustment used in the UGM and the global Euler models, but the boundary layer turbulence treatment is similar in all three models.

The final model is a global barotropic model designed to interpret results from the more complete models. Its' derivation is also described by Paegle (1989).

Global primitive equation model

Figure 3 displays the rms forecast wind sensitivity at sigma level .5 to the presence or absence of SALLJEX observations in the initial state. The results

are shown for selected forecast times and averaged for a series of predictions initialized at 06 UTC on 16 consecutive days starting on 15 January 2003. On forecast day 1 (upper left panel) the largest area of sensitivity is found over South America, as expected, and by days 9 (lower left) and 14 (lower right) the sensitivity spreads toward mid- and high-latitudes of each hemisphere.

Area integrations of rms forecast sensitivity were output at 12 h intervals. The resulting forecast averaged over selected domains is displayed in Fig. 4. The green curve represents forecast sensitivity averaged over a region from 80^0W-20^0W and 45^0S-Eq. This regional domain is centered on the field experiment. Here the sensitivity of the UGM prediction to SALLJEX observations declines slowly in the first week of forecasting and slowly increases in the second week. Globally and hemispherically averaged sensitivities show little evolution in the first seven days and weak, but steady increases during the second week. The regional behaviour in the first week of prediction is qualitatively similar to that found by Miguez-Macho and Paegle (2001) in mid-latitude winter-time forecast sensitivity experiments with the UGM. That study also found initially diminishing forecast sensitivity to locally targetted initial state changes. Higher resolution tests with the UGM suggest similar sensitivity shown in Fig. 3.

Global Euler Model

Figure 5 presents results analagous to those of Fig. 3 obtained with the global Euler model and Fig. 6 displays results similar to those of Fig. 4 for the global Euler model at 500 mb. The global Euler model clearly exhibits greater sensitivity to the presence of SALLJEX observations than does the UGM.

Regional Euler Model (WRF)

The WRF model integrations were performed every 12h for a duration of 48h. Figure 7 shows time series of the rms magnitude of the 500 mb wind difference between the control forecast and the experiment forecasts at 48h averaged over the domain of Fig. 1. The results displayed in Fig. 7 are in the same format as the time series of the analysis impact upon rms magnitude of wind difference shown in Fig. 2.

The differences at 48h are typically somewhat larger than those at the initial time. This is more clearly evident in Fig. 8 which displays the ratio of the forecast results of Fig. 7 divided by the initial differences in Fig. 2. Global primitive equation and Euler model sensitivities were calculated only for a sub-set of the WRF model cases presently displayed, including the interval of forecasts initialized from 15 January to 30 January, 2003. During this interval, the average 48h WRF forecast 500 mb wind sensitivity grows by approximately a factor of 1.1 from the initial time over its forecast domain, centered over South America; ie, about 10% average growth of initial state changes over 48h for the regional WRF forecasts. There is considerable variation in WRF forecasts sensitivity during this period. The largest percentage response to initial state changes ranges from about 25% to 40% during the particularly active weather period centered on 24 January.

The largest WRF wind sensitivity to SALLJEX observations occurs in the lower troposphere. Fig. 9 displays the ratio of forecast wind sensitivity to initial state sensitivity at 850 mb. At this level, the 48h forecast sensitivity

occassionally reaches or exceeds 200% of the initial state sensitivity, implying up to 100% growth over 48h. Over the last half of January, the average 850 mb WRF wind forecast sensitivity amplifies by approximately 50-60% over 48h.

It is interesting to compare WRF results with those of the global primitive equation and Euler models. The green curve of Fig. 4 displays the rms wind forecast sensitivity in the global primitive equation integrations performed during the last half of January, averaged over the domain centered on South America. This curve displays slow damping of initial state changes, on the order of 40% in the first 2 days of prediction with the UGM. By contrast, the analogous result for the global Euler model (green curve of Fig. 6 displays more than 200% average growth of the initial state wind differences over the South American sub-domain in the first two days of prediction.

The growth rates of the WRF model wind sensitivity are substantially larger than those observed in the first 48h of the UGM, but much smaller than those found in the same period in the global Euler model in similar sub-domains. The present results imply that the SALLJEX observations have slight, moderate, and strong forecast impact upon the global primitive equation model, the regional WRF model, and the global Euler model, respectively. The next section explores possible explanations.

5. Analysis of forecast sensitivity

We use a variable resolution version of the global Euler model to study the reasons for its forecast sensitivity to initial state detail over South America. The highest resolution portion of this model is centered over S. America. Here the resolution approaches that used in the WRF model, and the lowest resolution portion of the model is on the opposite side of the world, where the resolution is similar to that used in the earlier UGM and global Euler models outlined above. The variable resoution strategy allows interpretation of the high resolution WRF as well as the global models.

A brief summary of the variable resolution approach is presented here. More detail can be found in Paegle (1989), Wang et al. (1999), and Majcen (2005). The present model uses finite elements to approximate horizontal and vertical derivatives appearing in the forecast equations. The methods can be derived from Galerkin principles that have desirable conservation properties. Galerkin methods can also be used to obtain spectral techniques that are commonly used in global forecast models. The computational expense of spectral techniques increases with the fourth power of horizontal resolution. Spectral techniques consequently require (16, 81, 256) times as many calculations for (doubled, tripled, quadrupled) horizontal resolution.

Schmidt (1977) developed a spectral conformal transformation which has been used by Courtier et al (1991) and Hardiker (1997). This method requires substantially less calculation effort than uniform resolution spectral models for any given degree of locally maximized resolution, but the calculation burden still varies as the fourth power of resolution.

Finite element methods are more efficient than spectral methods and are accompanied by computational expense that varies with the third power of horizontal resolution in uniform mesh applications. The calculation burden

consequently increases by factors of (8, 27, 64) for (doubled, tripled, quadrupled) resolution.

Finite element methods are easily applied with variable resolution, and can therefore resolve much detail in important regions of the forecast domain, while more economical, lower resolution is used elsewhere. In the present application, the efficiency is further increased in the spherical coordinate system by rotating the mathematical pole to the area requiring increased horizontal resolution. The benefit associated with rotation of the pole toward the area of interest is that convergence of meridians ensures that modest angular resolution in longitude represents very high resolution in space near the pole in the east-west direction. Further resolution increases are consequently only required in latitude if interest is focused only upon an area sufficiently close to the pole. Consequently, the asymptotic calculation burden may increase only as the second power of resolution enhancement that is implied by increased latitude resolution and the need to satisfy the CFL stability criterion. The local calculation effort in the vicinity of the high resolution pole increases only by factors of (4, 9, 16) for locally (doubled, tripled, quadrupled) resolution.

Figure 10 presents the uniform distribution of grid points in a version of the model that has 82 points in latitude and 128 points in longitude, corresponding to latitude grid spacing of 2.22^0. This is the resolution for which the previously displayed global model results were obtained. Rotation of the model mathematical pole to a point located at 20^0S, 60^0 W provides the grid distribution shown in Fig. 11. Figure 12 shows a variable resolution grid in which the number of longitude grid circles remains 128, as in Fig. 11, while the number of latitude points is increased from 82 to 152, in an arrangement where the spacing of consecutive longitude circles increases by 1% per latitude circle outward from the high-resolution pole. The latitude resolution is about $.5^0$over most of Paraguay, Bolivia, and Argentina, degrading to 2.3^0at the opposite pole. The resolution over most of the region of the SALLJEX experiment is consequently quadrupled relative to the prior global Euler model experiments, and is now similar to that used in the regional WRF experiments, while the lowest resolution is similar to that used in the earlier global experiments.

The "grid-point" space projection in Fig. 12 emphasizes the region of interest. Half of the model grid points are used in the displayed region, and the other half are located over the remainder of the globe that is hidden from view. The total number of grid points has increased by a factor of 1.85 from Fig. 10 to Fig. 12 while the local resolution over South America is approximately quadrupled, but not degraded in remote portions of the globe.

The time step must be reduced by approximately a factor of 4, so the new calculations require about 4 X 1.85 or about 7.5 times as much computer time as the previous global integrations. Because of this, we next focus upon the first 5 days of prediction and describe only the preliminary case initialized on 00 UTC, 17 January. Our experiments emphasize the importance of horizontal diffusion and of precipitation processes.

We hypothesize that the relatively sensitive response of the global Euler model compared to the other currently tested models may be due partly to lack

of explicit horizontal diffusion on any of the forecast variables within the troposphere. Many other models include horizontal diffusion that acts most strongly on shortest scales, but, to a lesser extent, damps time changes in longer scales. In the case of the global UGM, this diffusion is explicitly included in second and fourth order methods (Paegle, 1989). The WRF model does not include horizontal diffusion explicitly, but it uses an up-wind biased advection scheme that retains a diffusive term (Wicker and Skamarock, 2002). The effective diffusion coefficient in the presently used version of the WRF model is proportional to the speed of the advecting wind.

By contrast, the current version of the global Euler model retains no explicit diffusion of resolved scales below 14 km. Above this level, the model includes horizontal diffusion of horizontal divergence, which is sometimes found necessary to control model noise near the upper boundary. Integrations of the variable resolution global Euler model initialized on 00UTC, 17 January using the present set-up suggest similar sensitivity to the presence or absence of SALLJEX observations in the initial state as that which occurs for the uniform resolution case. This can be seen comparing the green curve (variable resolution model sensitivity) and black curve (uniform resolution model sensitivity) of Fig. 13. This diagram displays time evolution of rms wind forecast sensitivity to the presence or absence of SALLJEX observations averaged over the region extending from 45^0S to the equator and from 80^0W to 20^0 W. The green and black curves are produced by identical parameterizations with models that differ only in resolution.

The variable resolution model shows an initially more rapid amplification of initial state differences than does the uniform resolution version, but the response is similar after approximately 4 days. After 48 h (on 19 Jan.) the variable resolution model amplifies the rms initial state sensitivity of 1 m/s to more than 5 m/s, corresponding to an increase of about 4 m/s, on the order of 400% of the initial state uncertainty for this case.

The yellow curve of Fig. 13 depicts forecast sensitivity when second order diffusion is included on wind and temperature forecasts of the variable resolution global Euler model. The diffusion coefficient is proportional to the square of the local grid size in the latitude coordinate multiplied by the local deformation rate. The response to the SALLJEX observations still amplifies in this case, but only by about a factor of 2 (ie, 100% amplification) after 48 h. This is considerably more than the response found in the WRF model (see Figs. 8 and 9) at the same time.

The computed forecast sensitivity is in a region centered in the summer subtropics that has considerable convective activity. The Euler model parameterizes convection via a convective adjustment scheme. We next describe how treatment of these model moist processes affects forecast sensitivity. The red curve of Fig. 13 displays the model sensitivity growth in a version that is integrated without condensation processes. The sensitivity evolution is weaker than in the full model integrations displayed by the black and green curves, but by 48h the initial state changes are nearly doubled in the present experiment.

We conclude that, although there is considerable variation in forecast re-

sponse to extra observations in the different experiments depicted in Fig. 13, they all exhibit sensitivity growth that is substantially larger than that found in the WRF model for forecasts initialized around 17 January (see Fig. 9). Although each of the present experiments suggest substantial forecast sensitivity, it is clear that versions with explicit diffusion and dry cases are less sensitive.

It is reasonable to hypothesize that models with stronger diffusion and ones that produce less precipitation would be less sensitive than presently described situations. We infer that the relatively strong global Euler model forecast response to initial state changes is due to weak effective diffusion and to large predicted precipitation rates. Comparison of precipitation predicted by this model and WRF suggest that the variable resolution global Euler model produces heavier rainfall than the WRF (not shown). It is also reasonable to suppose that forecast changes in regional experiments such as the WRF would be somewhat constrained by lateral boundary conditions.

In view of the impact of precipitation processes and diffusive mixing upon the forecast characteristics it is important to demonstrate that the parameterization of these processes in the variable resolution, global Euler model is reasonable. This is equivalent to demonstrating that the default treatment of moist processes (via convective adjustment) and of horizontal turbulent mixing (discarded below 14 km) does not produce a worse forecast than when moist processes are excluded and horizontal diffusion is added. Stated otherwise, the default model settings should not produce a model configuration that produces an amplifying forecast signal by amplifying erroneous and noisy components of the predicted fields.

One way to address this issue is to compare the objective performance of the predictions produced by various versions of the model. A preliminary step toward this goal is presented in the anomaly correlations calculated for the different variable resolution global Euler experiments. Figure 14 presents anomaly correlations for the precipitating case lacking tropospheric diffusion of resolved scales; Fig. 15 gives the result for the wet case with tropospheric diffusion; and Fig. 16 shows results for the dry case without tropospheric diffusion of resolved scales. The climatology for the anomaly correlations is taken from a 50-year (1951-2000) January average from the NCEP/NCAR Reanalysis. "Observations" are also from this reanalysis. A forecast with anomaly correlations in excess of .6 is generally considered to have sufficient skill to be useful for local prediction. The Southern Hemisphere curves of Fig. 14 maintain these levels through almost 144h, while the Northern Hemisphere skill is at this level for more than 120 h. By contrast, the cases with tropospheric diffusion and without precipitation exhibit at least 12h less skill in each hemisphere. This suggests that the version of the global Euler model upon which most of the present discussion is based is not unreasonably noisy and that the discussed sensitivities may not be mere artifacts of parameterizations.

Anomaly correlations for the UGM (PE model) were also computed for forecasts made for the same case. On a global basis, the results (not shown) are similar to those of the global Euler model, but the UGM has relatively greater accuracy in the Northern Hemisphere and relatively less accuracy in the South-

ern Hemisphere.

6. Summary and discussion

Model forecast response to new observations and observing systems provides one context in which to evaluate the observations. The central message of the present study is that conclusions from forecast sensitivity studies vary substantially between different models, different resolutions in a single model, and between experiments with a single model made with different parameterizations of horizontal mixing and precipitation. Much more study is required to determine which of the tested models is most accurate.

Prior studies have addressed the role of model diffusion and forecast detail. In particular, Skamarock and Baldwin (2003) emphasize the importance of limited diffusion in the WRF. They show that spectra of the horizontal structure of various weather elements is more realistic in the WRF model than in the Eta model and suggest that the WRF benefits from the relatively small amounts of horizontal diffusion.

Skamarock and Baldwin (2003) do not present point-by-point verification statistics of WRF forecasts. They state that "given this lack of formal predictability (of mesoscales) it can be expected that the more filtered (damped) forecasts will verify better using traditional verification methods". Our preliminary results neither contradict nor support this conclusion, and are based on only one case and one verification score.

In contrast to Skamarock and Baldwin's (2003) results, Knievel et al. (2005) find that the horizontal structure of selected WRF forecasts appears to improve when explicit 6th order horizontal diffusion is added in their implementation.

At present, we do not have clear-cut explanations for the enhanced sensitivity of the global Euler model relative to the WRF model. It is possible that the WRF model sensitivity to SALLJEX observations is inhibited by lateral boundary conditions, that are not present in the global Euler model. Less plausible possibilities relate to the use of time splitting methods to allow larger time steps in WRF. These methods are not used in the global Euler model. Detailed description of the WRF model is beyond our present scope, but that model appears to damp vertically integrated divergence, implying small vertical velocities near the model top. By contrast, the global Euler model uses effectively open top boundary conditions by imposition of zero vertical gradients (ie, $\partial(\ )/\partial z=0$) on all forecast variables, including w at the top of the model.

Each of these factors should be more systematically investigated, more cases should be executed with the variable resolution version of the global Euler model, and comparisons of model forecasts against local observations, including precipitation could be illuminating. It is also important to identify possible explanations of the strong reaction to SALLJEX experiments displayed in some of our experiments. As previously suggested, the highly responsive model configurations may simply amplify unrealistic components of a noisy forecast field. Although this was partly refuted in the previous section, the results of the global Euler model would be more credible if a simpler, commonly accepted antecedent model were to illustrate similar sensitivity to initial state variations.

Prior predictability theories have emphasized the roles of barotropic insta-

bility (Lorenz, 1972), baroclinic instability (Tribbia and Baumhefner, 2004, and references therein) and phase sensitivity associated with uncertain advection rates (Thompson, 1957, Miguez-Macho and Paegle, 2000). Among these three possibilities, barotropic instability has probably seen the least recent emphasis. Advection errors would be most obvious in the presence of large-scale initial state perturbations (Miguez-Macho and Paegle, 2000), rather than the smaller-scale modifications due to SALLJEX observations. Baroclinic instability should favor synoptic scale waves and be most conspicuous in mid- and high-latitudes of the winter hemisphere. Baroclinic instability may consequently not explain the sensitivity found in the tropics and subtropics at day 4 in Fig. 5.

The final experiment re-visits the potential role of barotropic instability. Figure 17 presents rms wind sensitivity to the presence or absence of SALLJEX observations in barotropic integrations. These integrations are performed using single-level, non-divergent barotropic versions of the UGM described by Paegle (1989), on a 512X361 global longitude-latitude grid. The global grid spacing is similar to the local spacing used in the WRF integrations. The integrations were performed at 500 mb and at 200 mb, and sensitivity results of Fig.17 pertain to these levels and are displayed as global averages as well as regional averages centered on the SALLJEX experiment. The model has no horizontal diffusion, and it conserves globally integrated kinetic energy to within approximately 2% of the initial value.

The black and green curves of Fig. 17 display regional sensitivity in the barotropic model at 200 mb and 500 mb, respectively. They can be compared to the red curve of Fig. 13 which displays the 500 mb regional sensitivity of the variable resolution global Euler model run in a dry, frictionless version. The latter shows an increase from about 1 m/s to almost 4 m/s after 5 days. This sensitivity lies between the regional sensitivities displayed at 200 mb and 500 mb in the barotropic integrations of Fig. 17.

The result is consistent with the possibility that barotropic instability of the upper troposphere generates amplifying sensitivity to SALLJEX observations, and the sensitivity propagates vertically to other levels in the variable resolution global Euler model, where it is further amplified by moist processes. Although this provides one possible explanation for the strong response to SALLJEX observations in the global Euler model, it is unclear why the same mechanism is not equally evident in the WRF and global PE models. Our investigation of this problem continues with emphasis on the roles of horizontal diffusion, convective processes, and limited area vs global methodologies.

7. References

Byerle, L. A. and J. Paegle, 2004: Diagnosis of medium-range predictability enhancement during anomalous winter zonal flows over western North America. *J. Geophys. Res.*, **109, D17101, doi:10.1029/2004JD004736.**

Courtier, P., Freydier, C., Geleyn, J. F., Rabier, F., Rochas, M.: 1991: The ARPEGE project at METEO-FRANCE, in *Proceedings of the ECMWF Seminar, vol II,* pp 193-231, Eur. Cent. For Medium-Range Weather Forecasts, Geneva.

Dirceu, H., V. E. Kousky, and W. Ebisuzaki, 2007: The impact of high-

resolution SALLJEX data on NCEP global analysis. *J. Climate*, in press.

Hardiker, V., 1997: A global numerical weather prediction model with variable resolution, *Mon. Wea. Rev.*, **125**, 59-73.

Knievel, J. C., G. H. Bryan, and J. P. Hacker, 2005: The utility of 6th-order, numerical diffusion in the Advanced Research WRF Model. *Proceedings of the WRF/MM5 Users' Workshop*, June 2005.

Lorenz, E. N., 1969: The predictability of a flow which possesses many scales of motion. *Tellus*, **21**, 289-307.

Lorenz, E. N., 1972: Barotropic instability of Rossby wave motion. *J. Atmos. Sci.,* **29**, 258-264.

Majcen, M., 2005: SALLJEX forecast experiments with a global variable resolution model. Master's thesis, University of Utah, 125 pp.

Miguez-Macho, G. and J. Paegle, 2000: Sensitivity of a global forecast model to initializations with reanalysis data sets. *Mon. Wea. Rev.*, **128**, 3879-3889.

Miguez-Macho, G. and J. Paegle, 2001: Sensitivity of North American numerical weather prediction to initial state uncertainty in selected upstream subdomains. *Mon. Wea. Rev.*, **129**, 2005-2022.

Paegle, J., 1989: A variable resolution global model based upon Fourier and finite-element representation. *Mon. Wea. Rev.*, **117**, 583-606.

Roman, J. C., G. Miguez-Macho, L. A. Byerle, and J. Paegle, 2004: Intercomparison of global research and operational forecasts. *Wea. and Fcsting.,* **19**, 534-551.

Roman, J. C., 2004: Intercomparison of global research and operational forecasts. Doctoral thesis, University of Utah, 111 pp.

Skamarock, B. and M. Baldwin, 2003: An evaluation of filtering and effective resolution in the WRF mass and NMM dynamical cores. draft manuscript

Thompson, P. D., 1957: Uncertainty of initial state as a factor in the predictability of large-scle atmospheric flow patterns. *Tellus*, **9**, 275-295.

Tribbia, J.J., and D. P. Baumhefner, 2004: Scale interactions and atmospheric predictability: an updated perspective. *Mon. Wea. Rev.*, **132**, 703-713.

Vera, C., J. Baez, M. Douglas, C. B. Emanuel, J. Marengo, J. Meitin, M. Nicolini, J. Nogues-Paegle, J. Paegle, O. Penalba, P. Salio, C. Saulo, M. A. Silva Diasm, and E. Zipser, 2006: The South American low-level jet experiment. *Bull. Am. Meteo. Soc.*, **87**, 63-77.

Wang, M., J. Paegle, and S. P. DeSordi, 1999: Global variable resolution simulations of Mississippi River basin rains of summer 1993. *J. Geophys. Res.*, **104**, 19, 399-19,414.

Wicker, L. J. and W. C. Skamarock, 2002: Time-splitting methods for elastic model using forward time schemes. *Mon. Wea. Rev.*, **130**, 2088-2097.

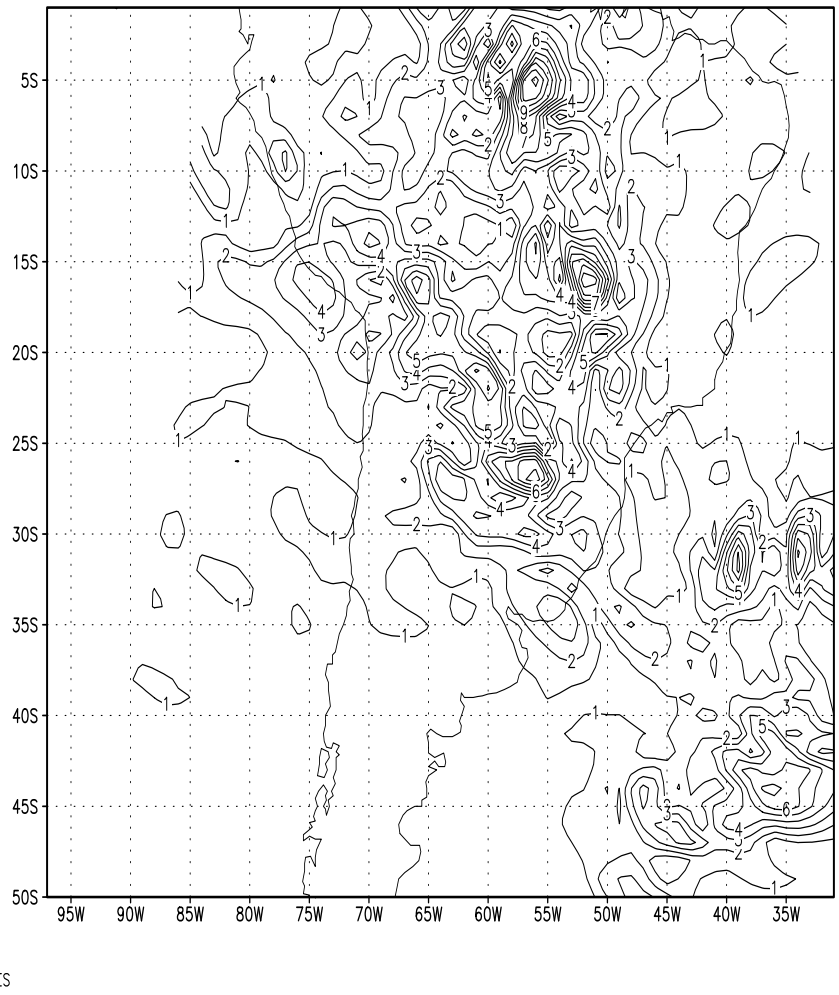

Figure 1: Magnitude of 500 mb wind difference between control and experiment analyses at 00 UTC 24 January 2003. Contour interval is 1 m/s.

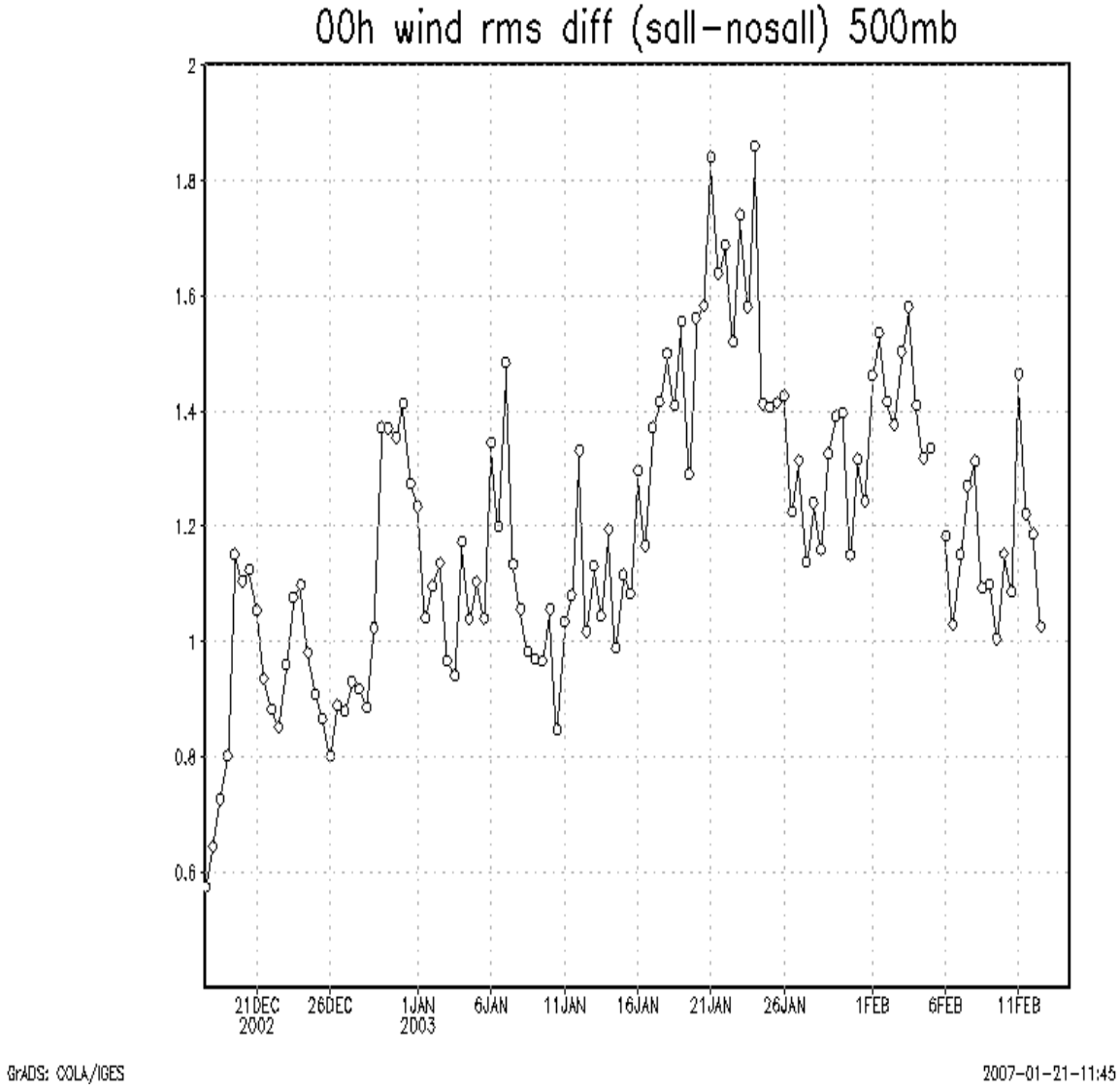

Figure 2: Time series of rms magnitude of the wind difference (in m/s) between control and experiment 500 mb wind analyses averaged over domain of Fig. 1.

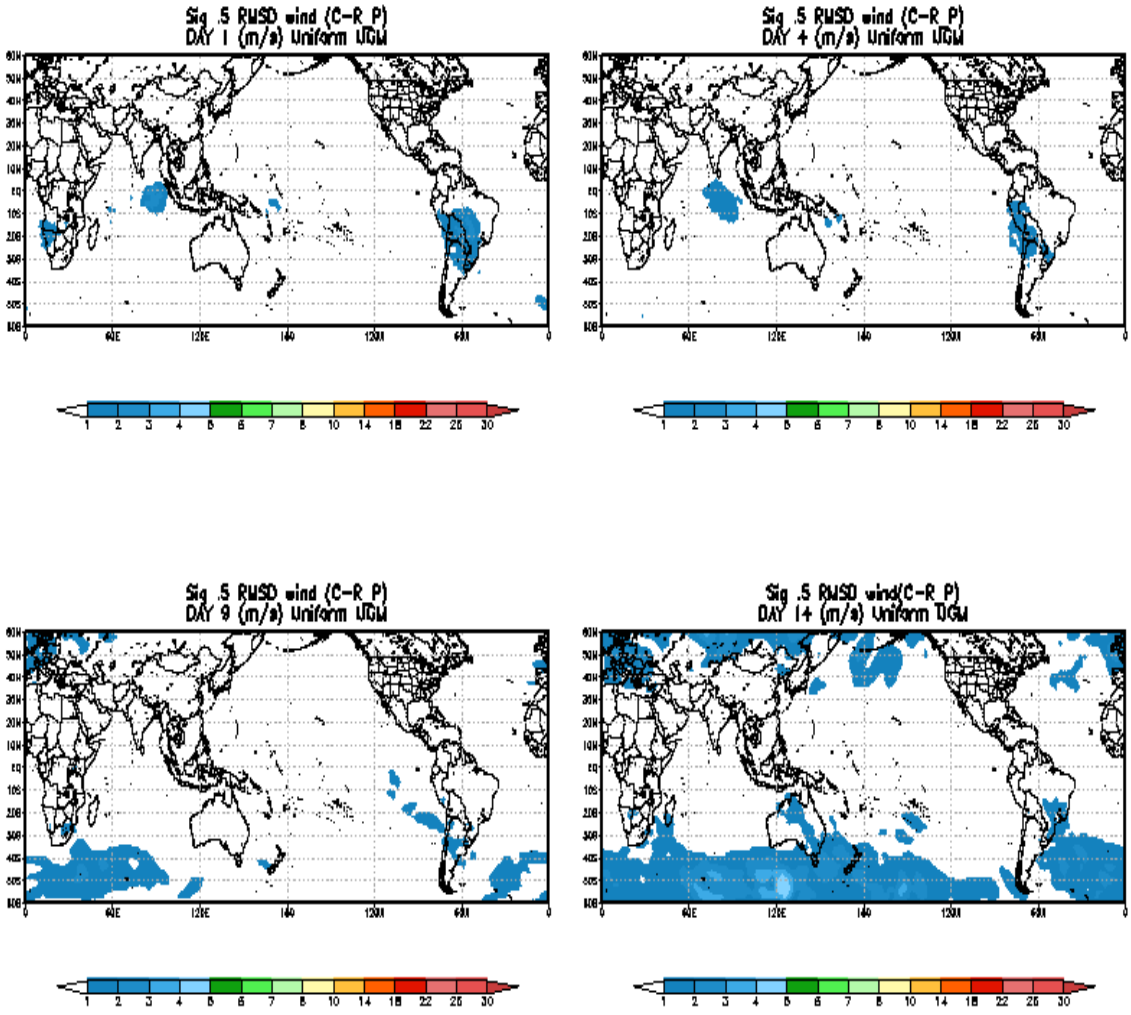

Figure 3: Root mean square difference (m/s) between sigma .5 wind forecasts made by the UGM using experiment initial states and UGM forecasts using control initial states. Day 1 (upper left), day 4 (upper right), day 9 (lower left), and day 14 (lower right) forecast times are displayed.

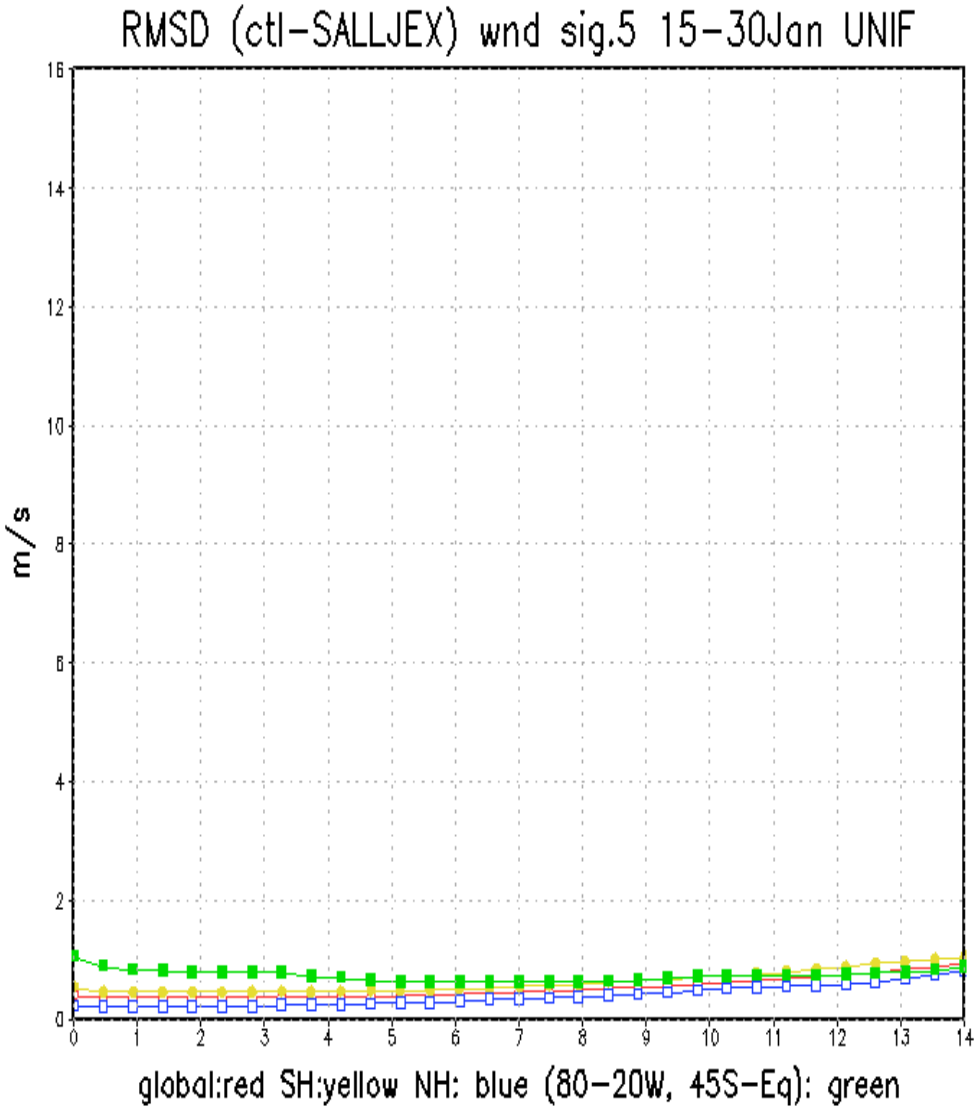

Figure 4: Time evolution of area integrated rms sensitivity between sigma .5 wind forecasts made by the UGM using experiment intitial states and UGM forecasts using control initial states. The red curve (open circles) represents globally averaged sensitivity, yellow (solid circles) and blue (open boxes) curves represent averages over southern and northern hemisphere, respectively, and the green curve (solid boxes) is an average over a domain centered on South America.

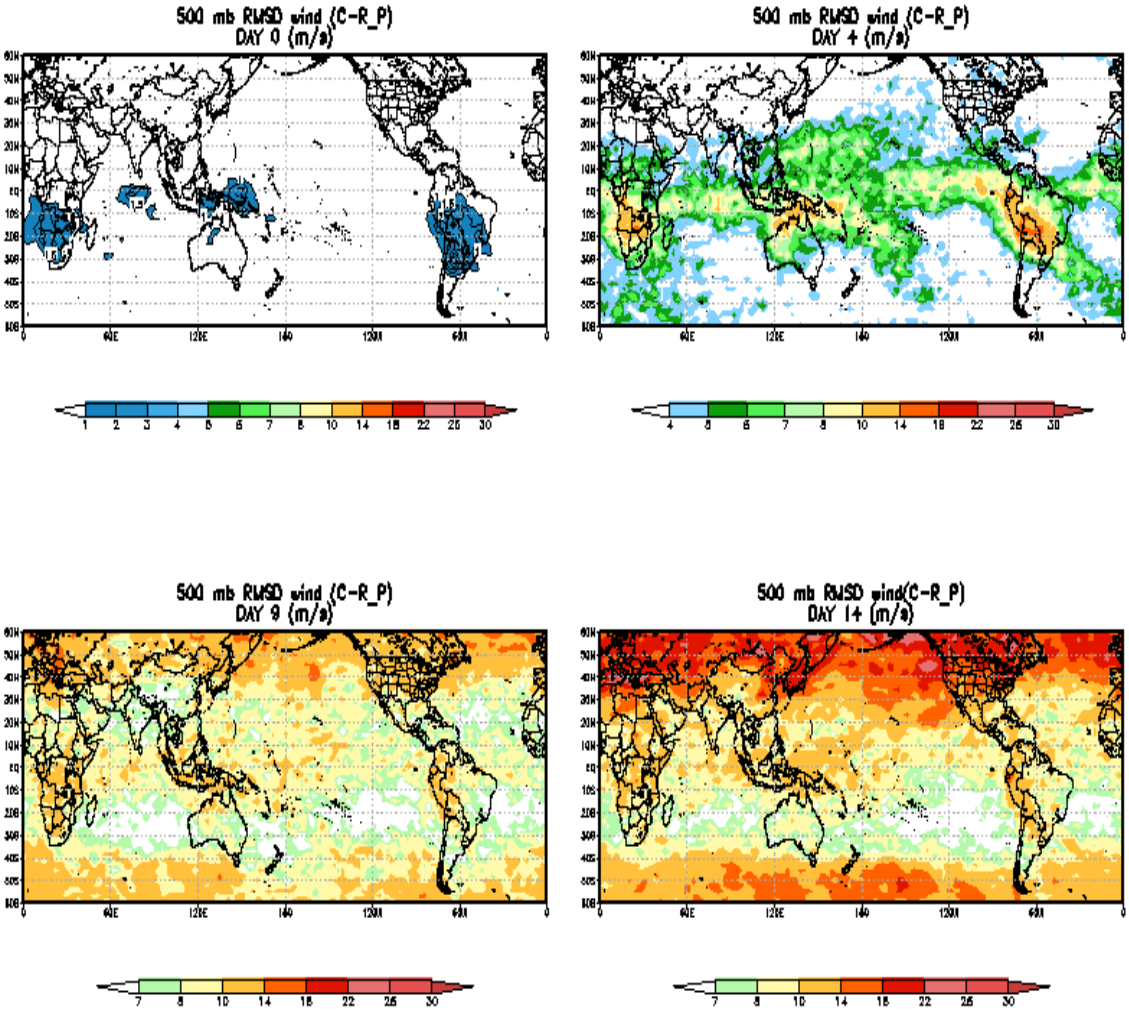

Figure 5: Root mean square difference (m/s) between 500 mb wind forecasts made by the global Euler model using experiment initial states and global Euler model forecasts with control initial states. Day 0 (upper left), day 4 (upper right), day 9 (lower left), and day 14 (lower right) forecast times are displayed.

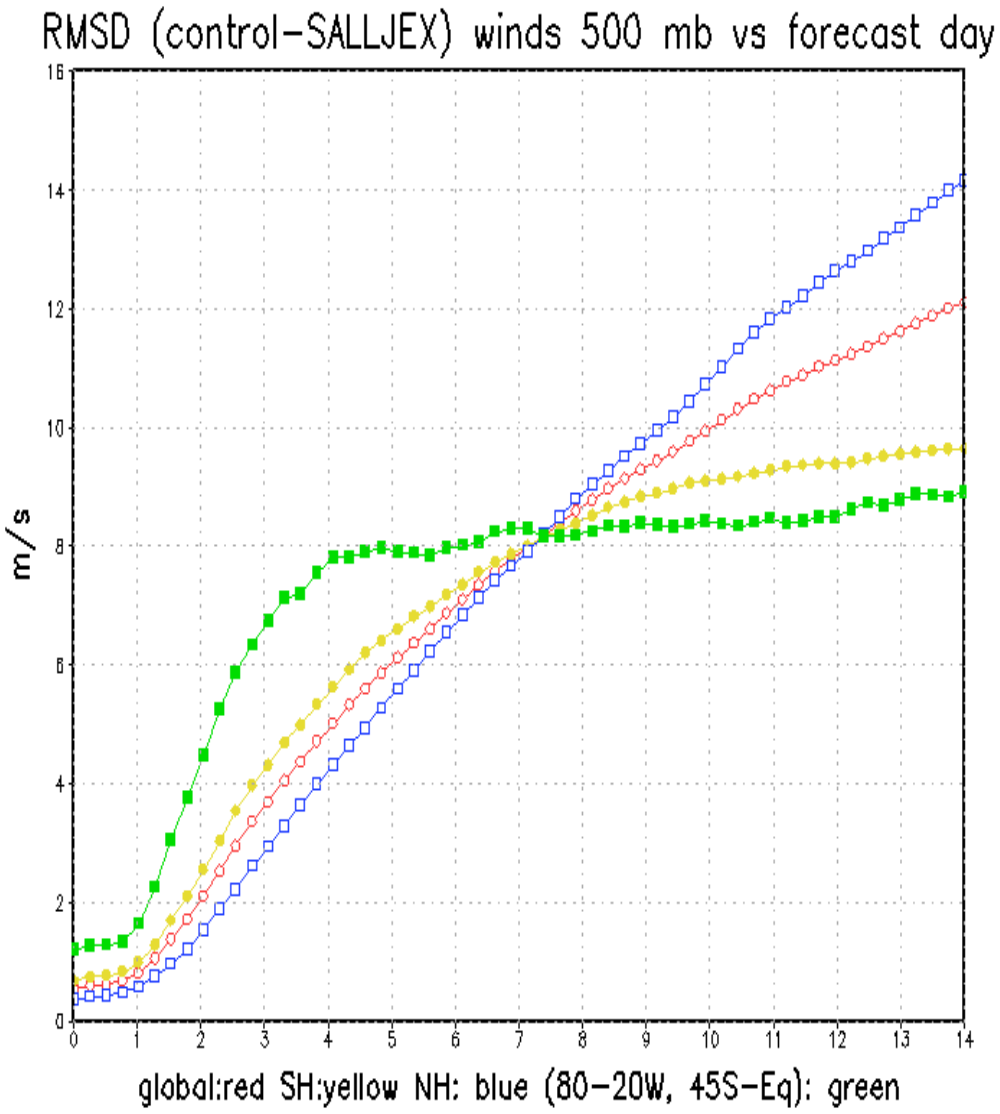

Figure 6: Time evolution of area integrated rms sensitivity between 500 mb wind forecasts made by the global Euler model using experiment initial states and global Euler forecasts using control initial states. The red curve (open circles) represents globally averaged sensitivity, yellow (solid circles) and blue (open boxes) curves are averages over southern and northern hemisphere, respectively, and the green curve (solid boxes) is an average over a domain centered on South America.

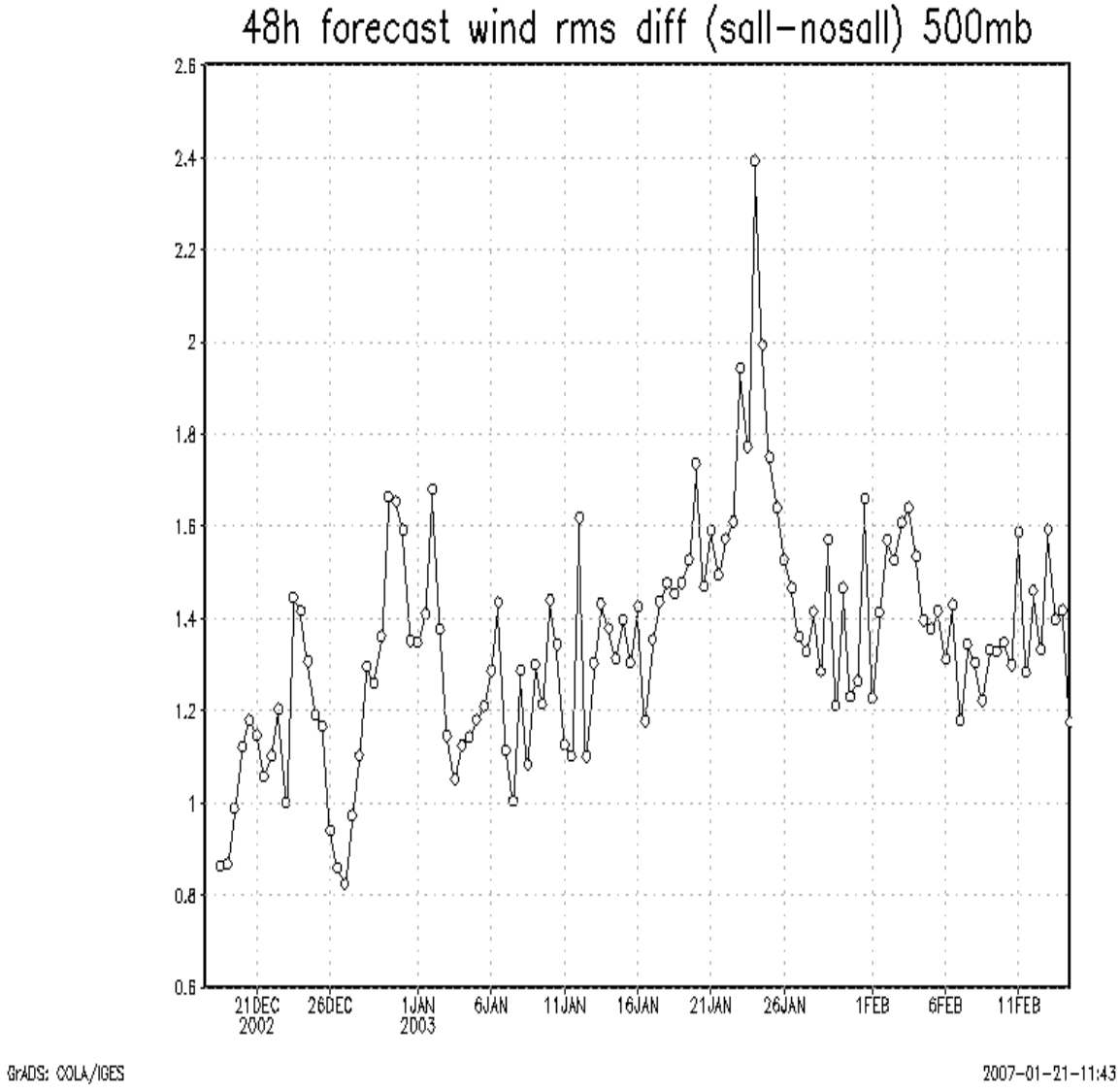

Figure 7: Time series of 500 mb wind difference (in m/s) between the control forecasts and the experiment forecast at 48 h by the WRF model.

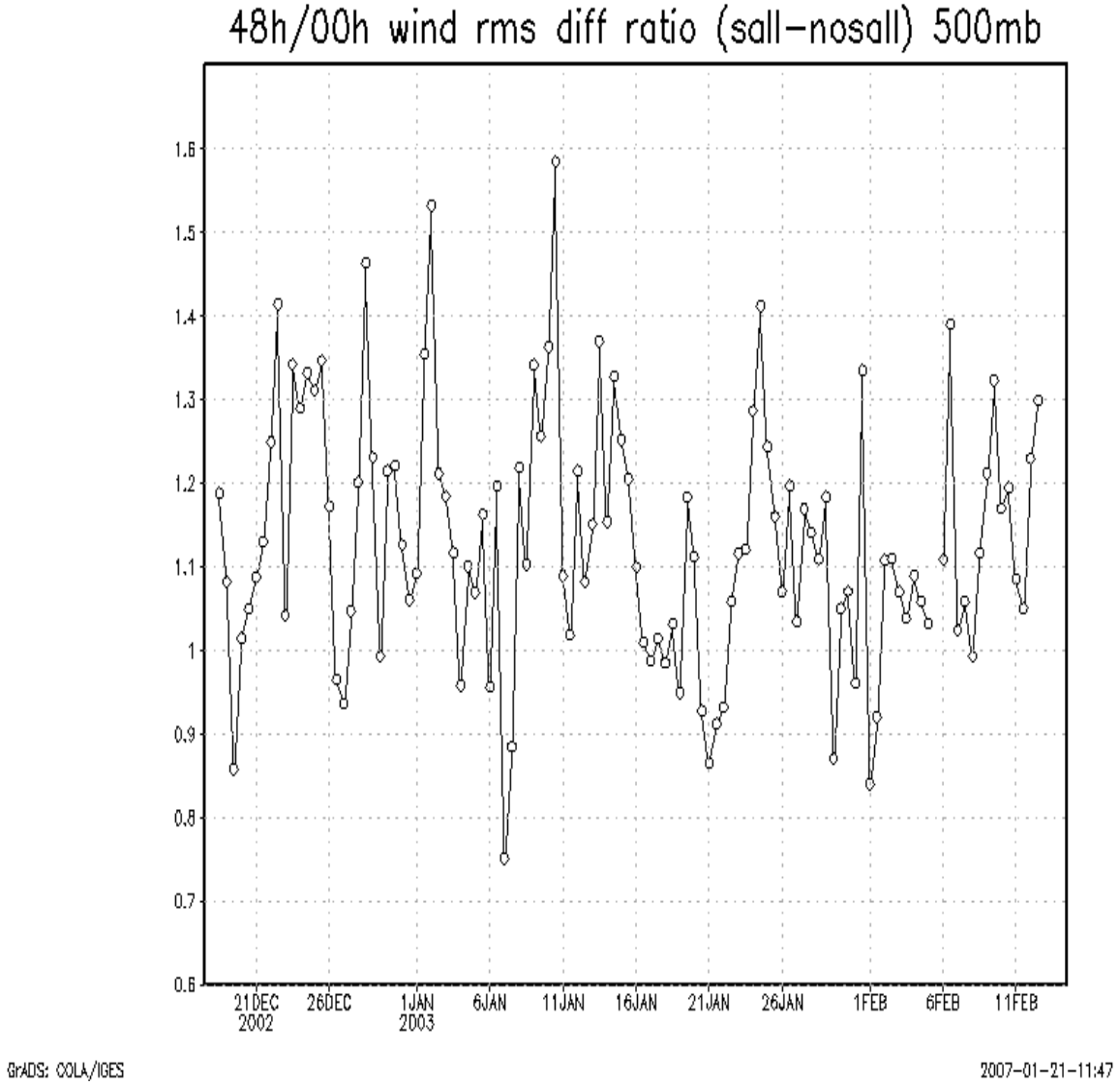

Figure 8: Ratio of 48h WRF model forecast wind sensitivity displayed in results of Fig. 7 divided by initial state wind sensitivity displayed in Fig. 2

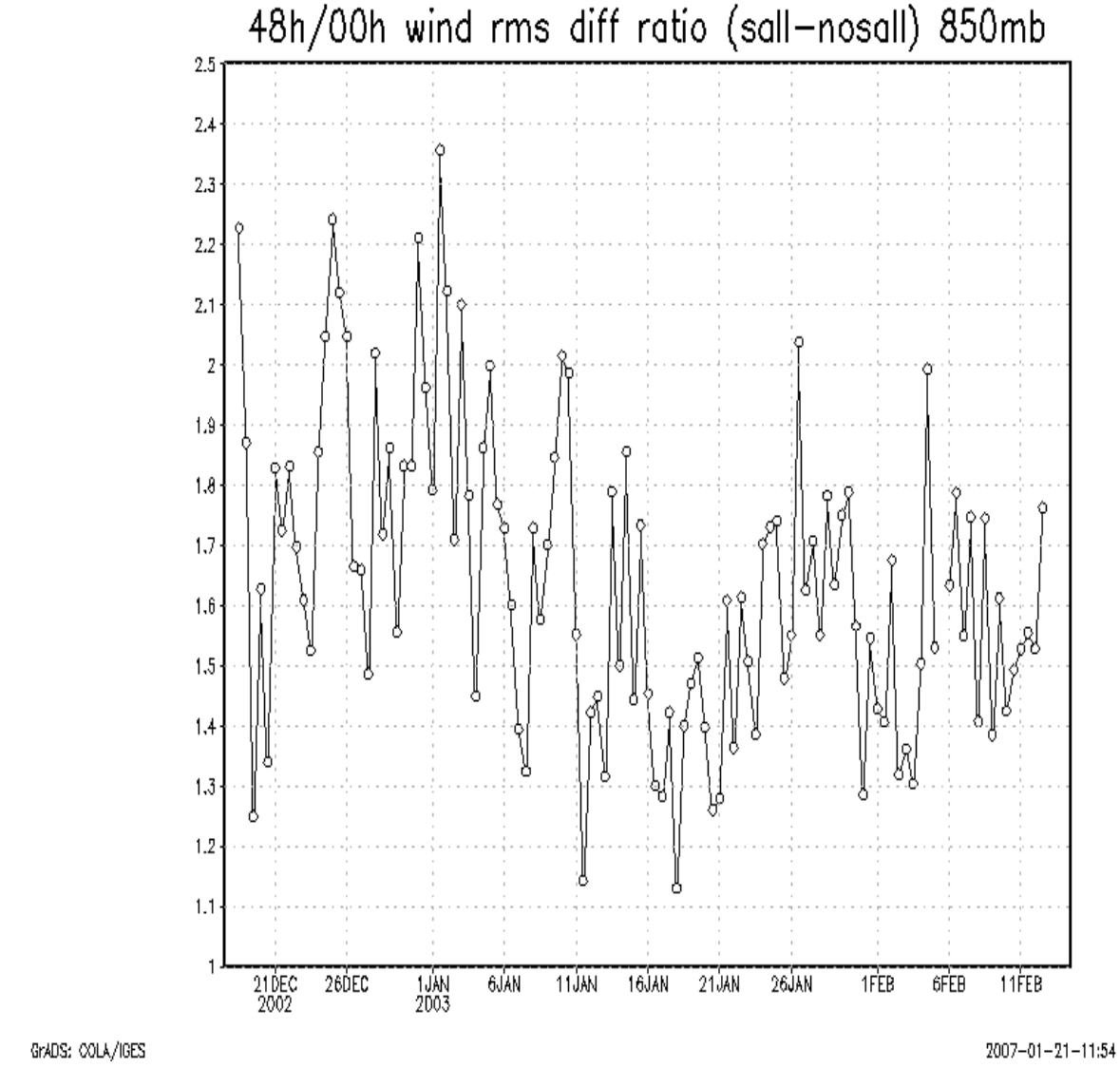

Figure 9: Ratio of rms 48h WRF model forecast wind sensitivity divided by initial wind sensitivity at 850 mb averaged over domain shown in 1.

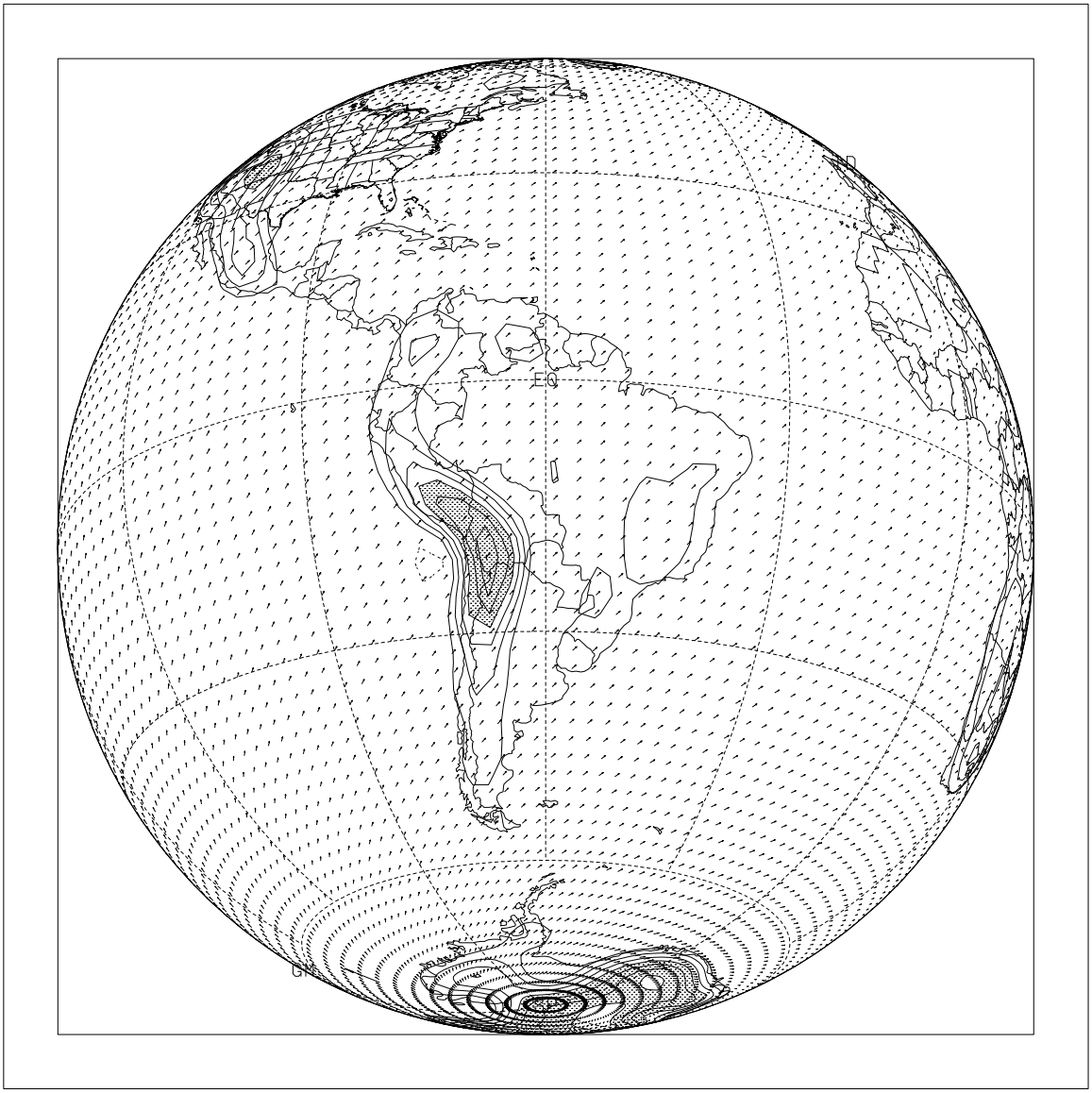

Figure 10: Location of model grid for a mesh on uniformly spaced 128 longitude circles and 82 latitude circles with the model poles at the geographical pole.

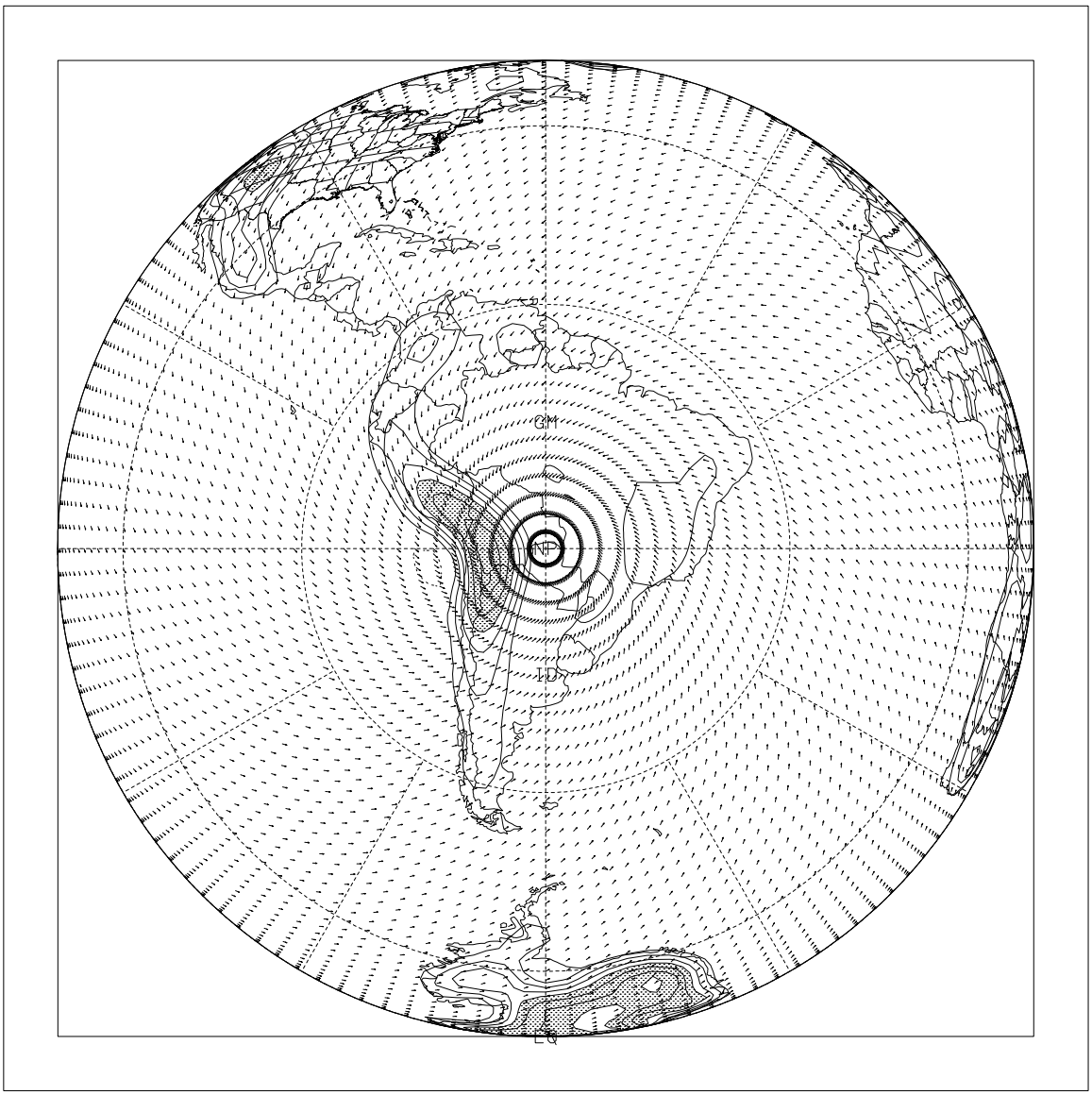

Figure 11: Rotated 128X 82 model grid with pole centered at 60 ^{0}W, 20^{0}S.

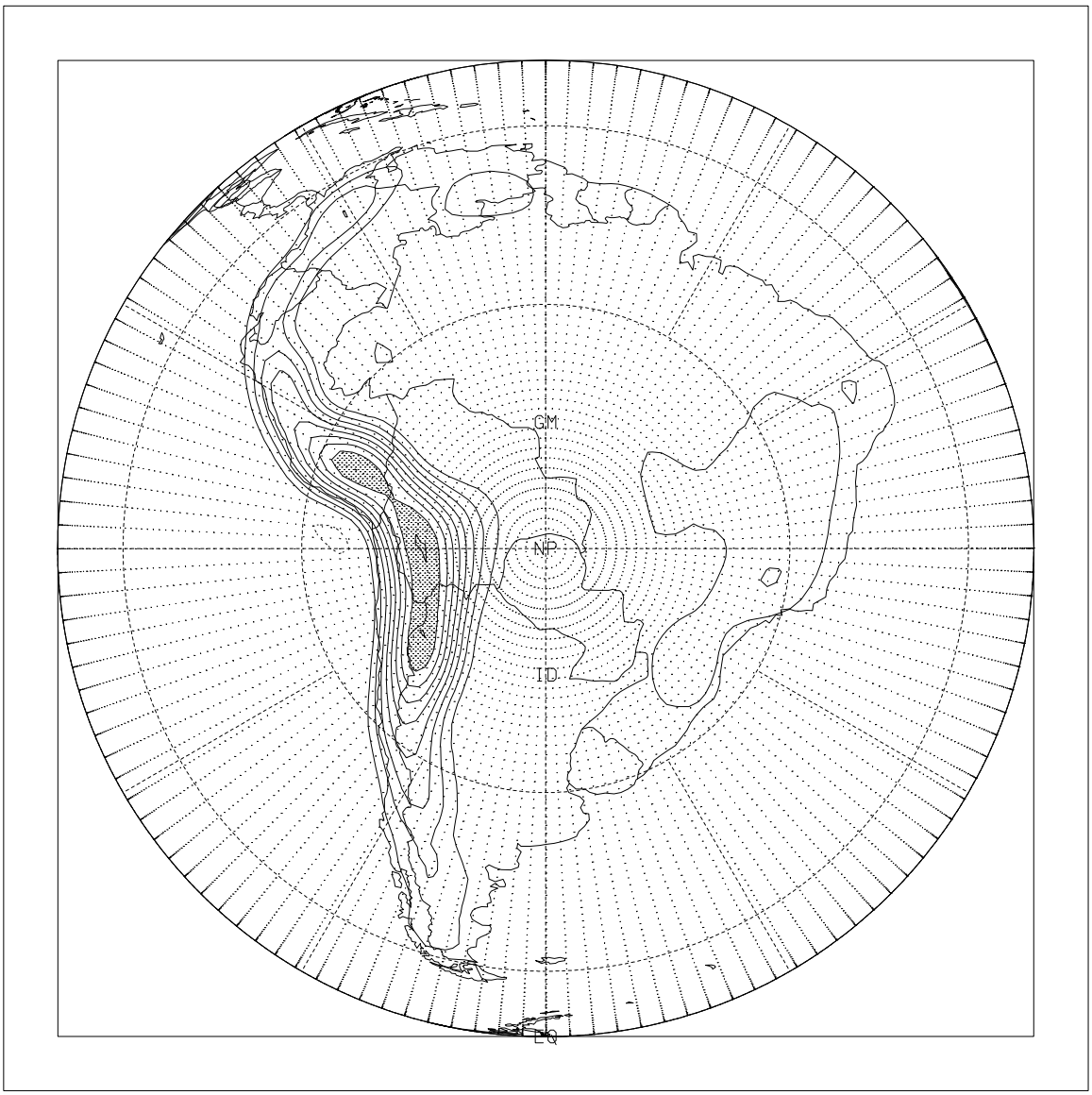

Figure 12: Variable resolution mesh with 128X152 grid points.

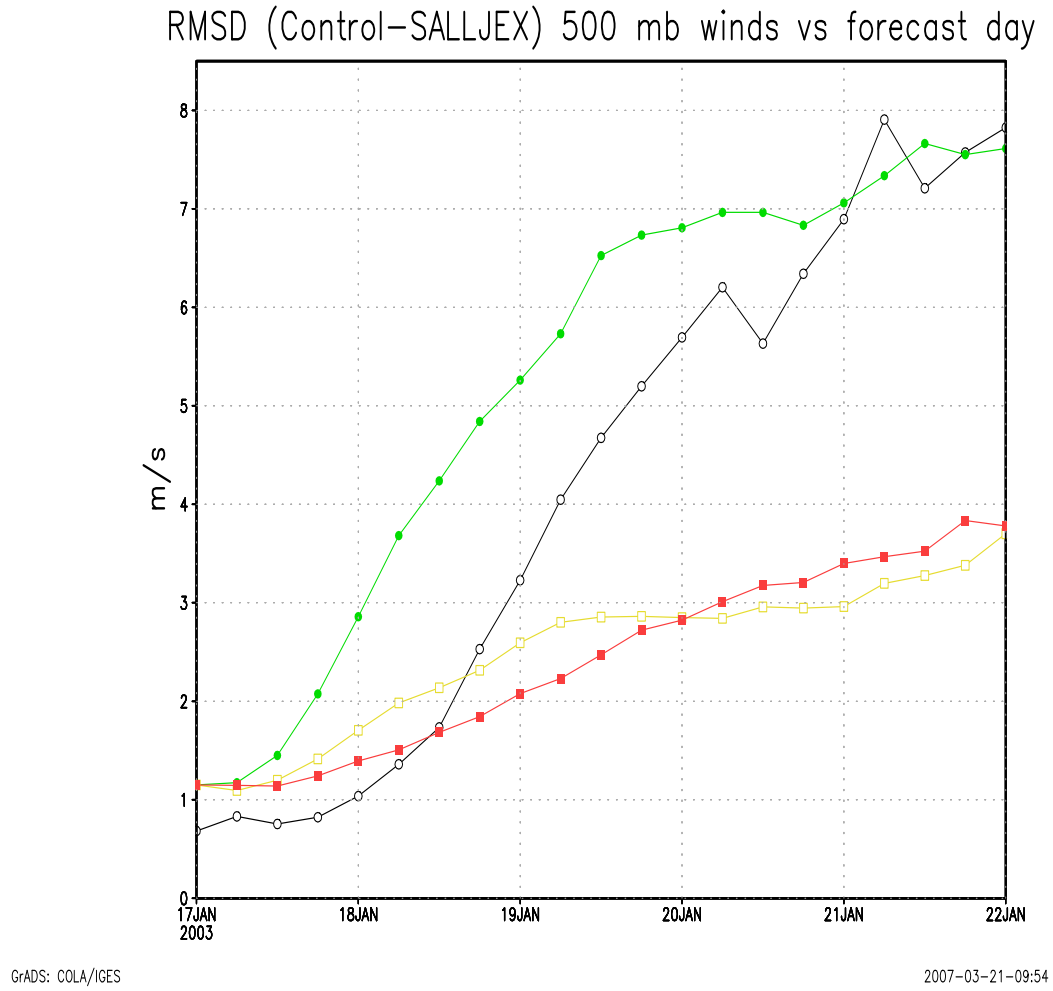

Figure 13: Time evolution of area integrated rms sensitivity between 500 mb wind forecasts made by the variable resolution global Euler model forcasts using experiment initial states and forecasts using control initial states. Green curve (solid circles) is precipitating case without explicit horizontal diffusion in the troposphere. Yellow curve (open boxes) is precipitating case with second order horizontal diffusion for wind and temperature forecasts. Red curve (solid boxes) is dry case without without explicit tropospheric horizontal diffusion. Black curve (open circles) is for earlier, uniform resolution version on 128 X 82 grid.

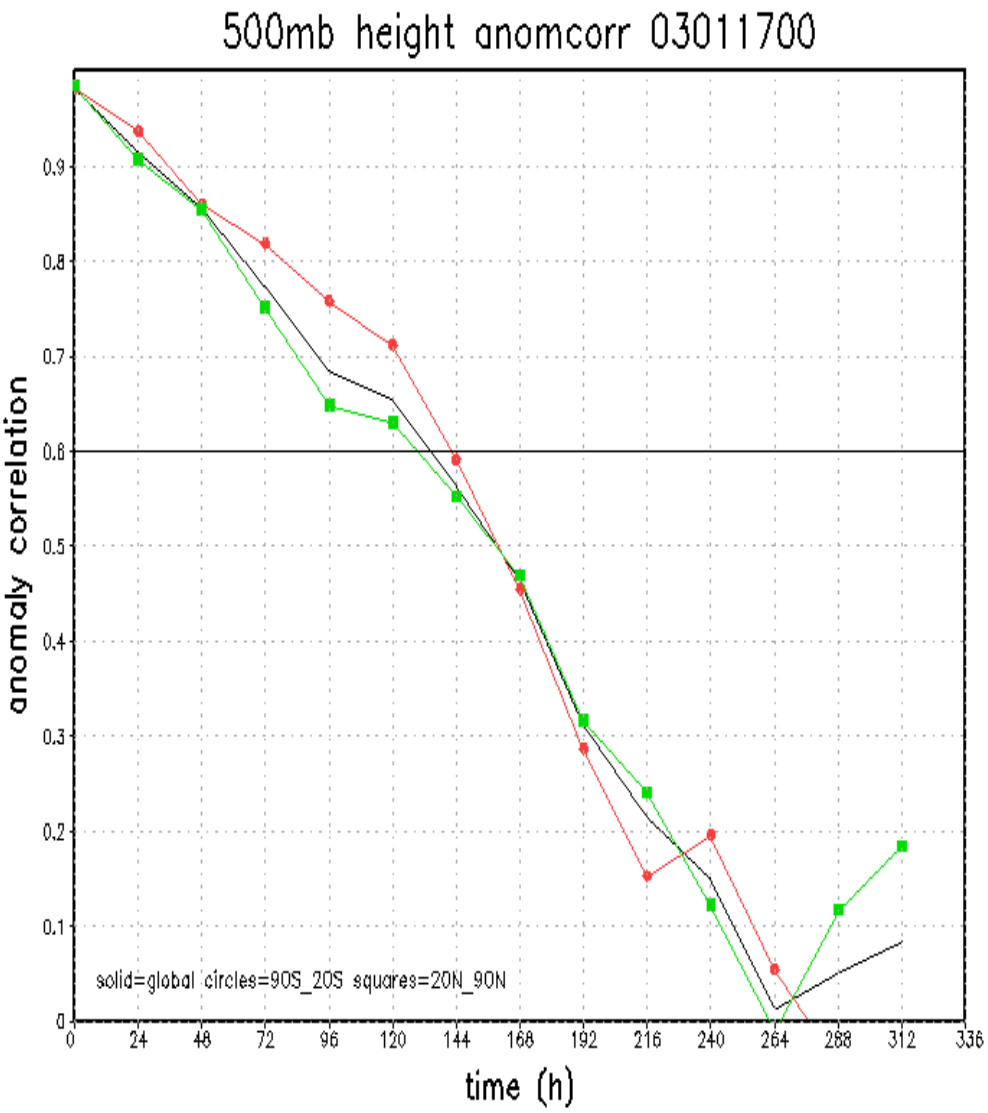

Figure 14: Anomaly correlations for forecasts of variable resolution model for the globe (black curve), 20^0N to 90^0N (green curve with boxes), and 90^0S to 20^0S (red curve with circles). Results are for the precipitating case without explicit horizontal diffusion in troposphere.

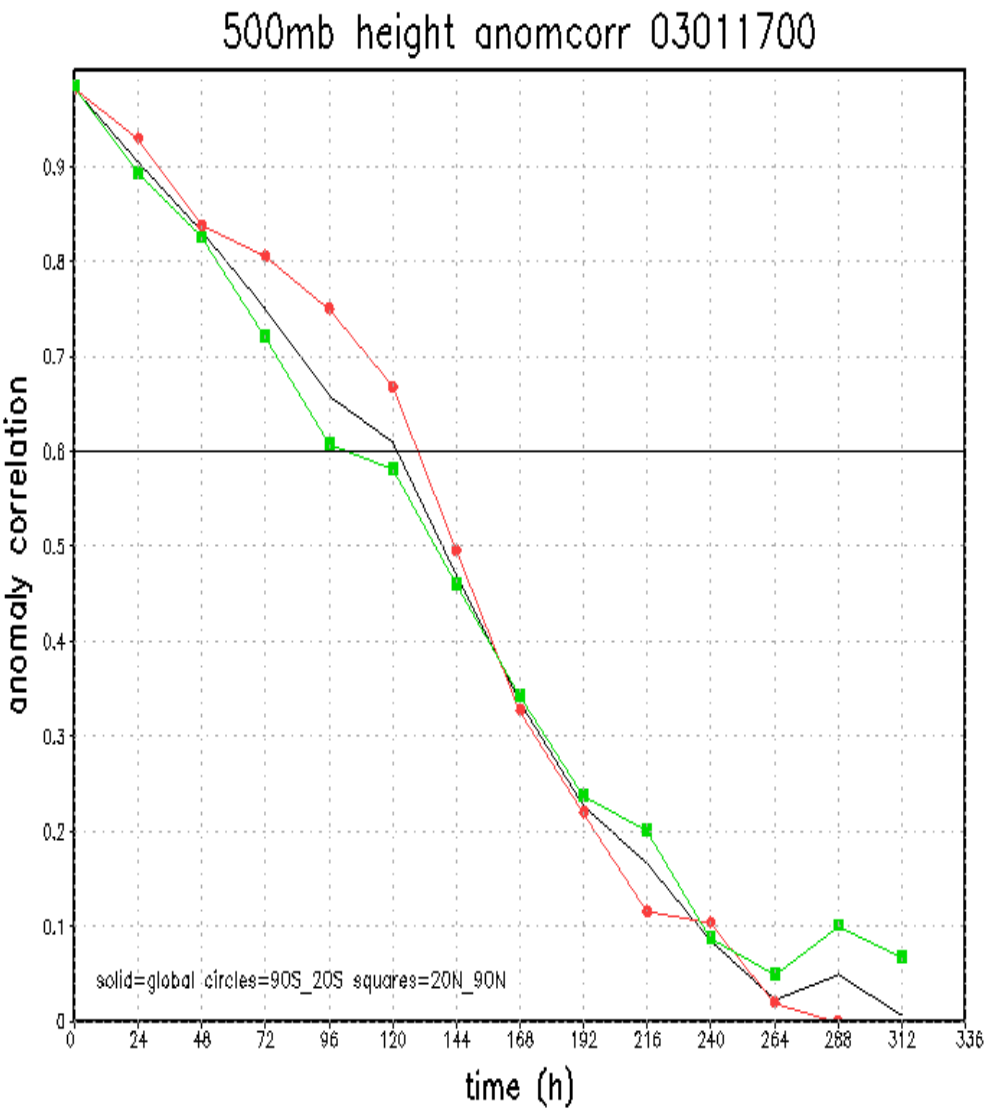

Figure 15: Anomaly correlations for forecasts of variable resolution model for the globe (black curve), 20^0N to 90^0N (green curve with boxes), and 90^0S to 20^0S (red curve with circles). Results are for the precipitating case with explicit horizontal diffusion of wind and temperature.

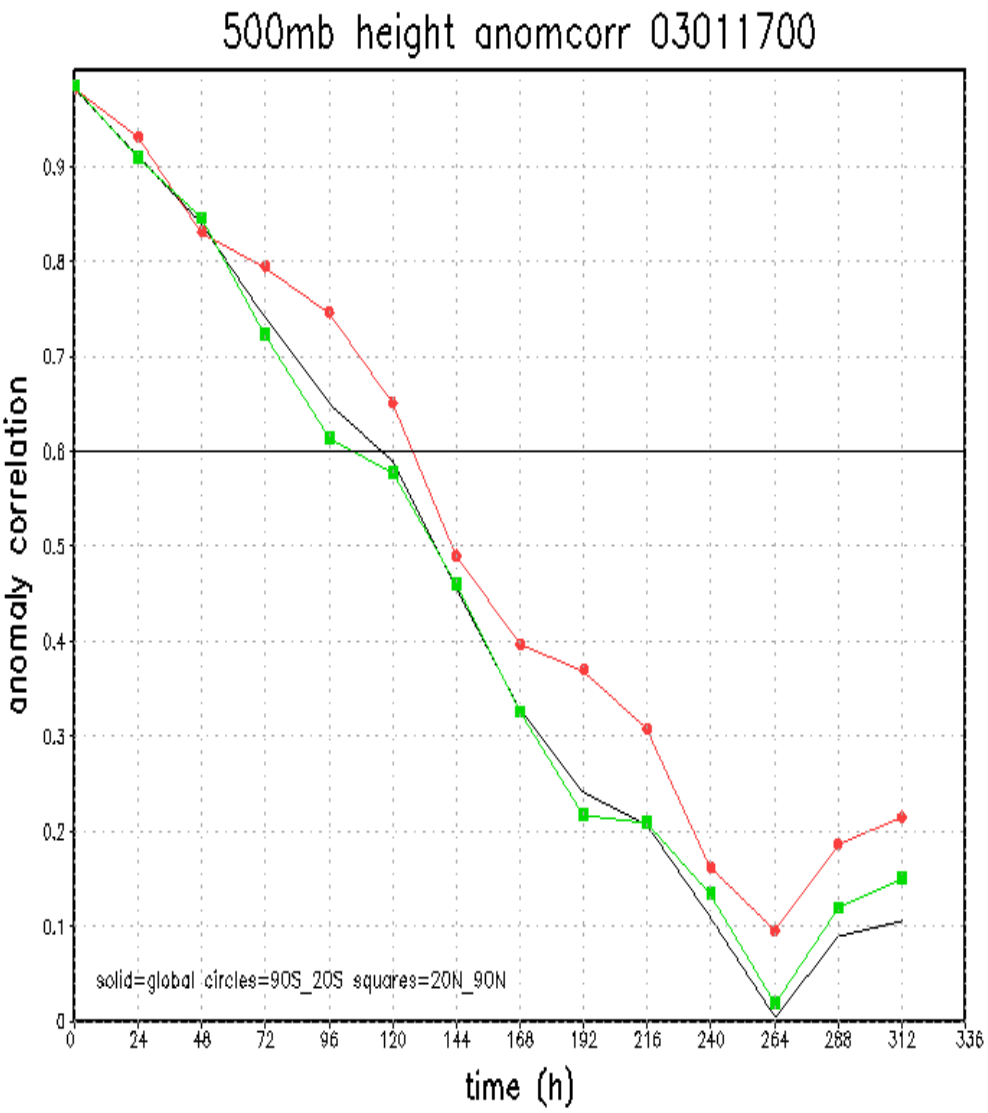

Figure 16: Anomaly correlations for forecasts of variable resolution model for the globe (black curve), 20^0N to 90^0N (green curve with boxes), and 90^0S to 20^0S (red curve with circles). Results are for the dry case without explicit horizontal diffusion in troposphere.

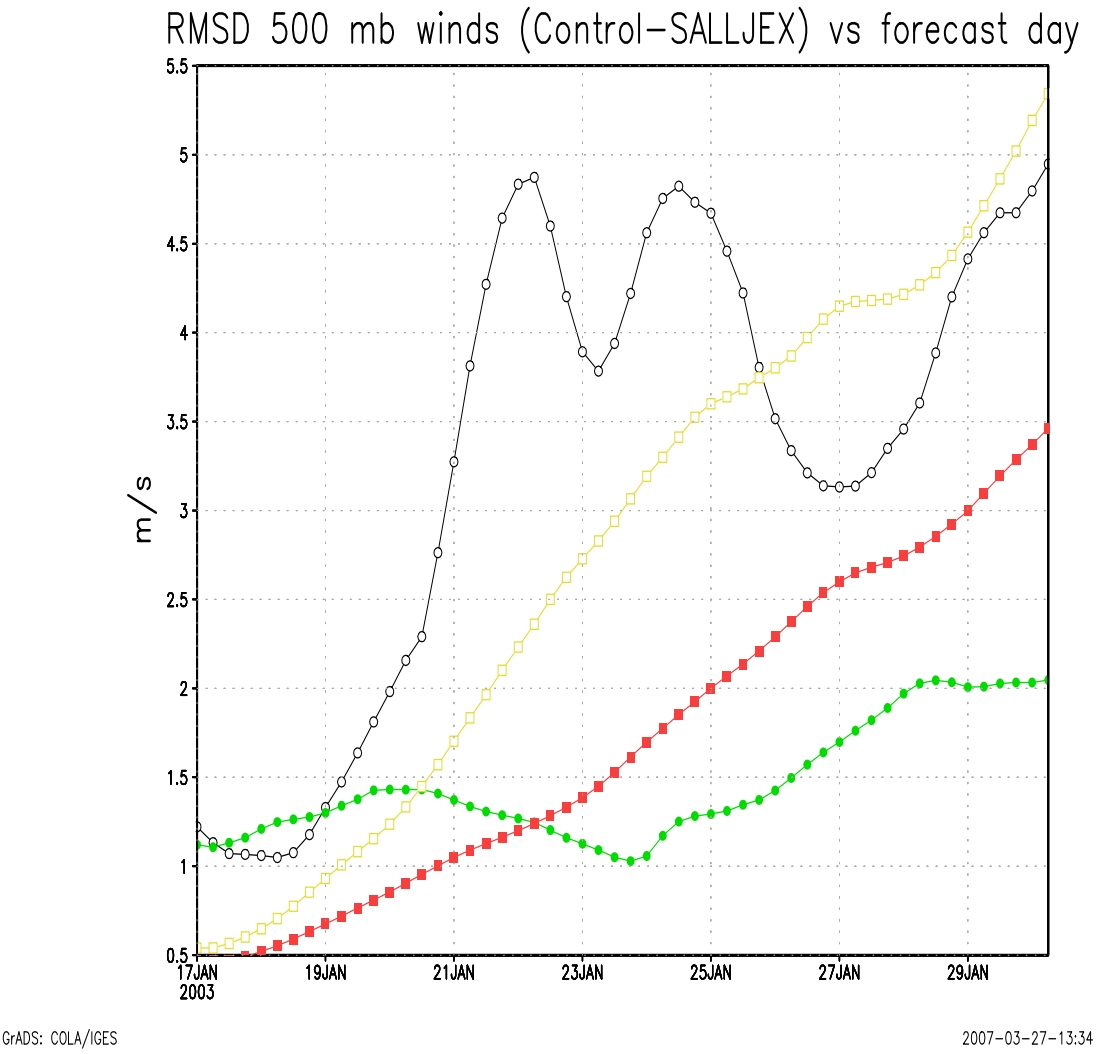

Figure 17: Sensivivity of barotropic model wind forecasts to SALLJEX observations. Black curve (open circles) for 200 mb averaged over (80^0W-20^0W, 45^0S-Eq). Green curve (solid circles) for 500 mb averaged over (80^0W-20^0W, 45^0S-Eq). Yellow curve (open boxes) for 200 mb, globally averaged, red curve (solid boxes) for 500 mb globally averaged.